An experimental study of a volatiles distributor for solid fuels chemical-looping combustion process

Fuel Processing Technology 220 (2021) 106898

Contents lists available at ScienceDirect

Fuel Processing Technology

journal homepage: www.elsevier.com/locate/fuproc

An experimental study of a volatiles distributor for solid fuels chemical-looping combustion process

Xiaoyun Li *, Anders Lyngfelt, Tobias Mattisson

Division of Energy Technology, Department of Space, Earth and Environment, Chalmers University of Technology, 412 96 Gothenburg, Sweden

ARTICLE INFO

Keywords:
Volatiles distributor
Chemical-looping combustion
Solid fuels
Gas-solid contact

ABSTRACT

A novel concept called volatiles distributor (VD), with the purpose to achieve an even distribution of volatiles over the cross-section of a fluidized-bed and better contact between volatiles and bed materials, has been investigated. The concept could be useful for chemical- looping combustion, as well as other solid fuel conversion processes in fluidized-beds. An experimental study of the VD in a circulating fluidized-bed (CFB) cold-flow model was conducted under different fluidization velocities and flows of simulated volatiles. In the reference case without VD, a local plume of volatiles is formed and the maldistribution becomes more pronounced at higher fluidization velocity in the range from 1 m/s to 4 m/s. Conversely, higher fluidization velocity gives a more even volatiles distribution in the presence of VD. The relative standard deviation of volatiles horizontal distribution decreases from 131% in absence of VD to 22% in presence of VD at the fluidization velocity of 4 m/s. There is no significant effect of volatiles flow rate on VD performance at a fluidization velocity 1 m/s. As the fluidization velocity and volatiles flow rate increase, the bed level inside VD is lowered and the volatiles inside the VD become less diluted, because less air from the main fluidization passes through the VD.

1. Introduction

Chemical-looping combustion (CLC) separates conventional combustion into two steps, avoids the direct contact between fuel and air, and allows for inherent CO_2 separation. Thus, CLC has potential for a significant breakthrough in carbon capture and storage area in order to alleviate climate change. Since the CLC concept was coined in 1987, it was initially developed for gaseous fuels [1]. Gradually, its application was extended to solid fuels like coal, since solid fuels are still the major energy source in the medium-term all over the world. Lately, the use of biomass in CLC is receiving increasing interest. Chemical-looping combustion of biomass together with the CO_2 capture and storage process can give negative CO_2 emissions because the captured CO_2 originates from the atmosphere through the photosynthesis of plants.

It will be difficult or perhaps even impossible to meet the Paris Agreement's temperature goal only by reducing greenhouse gas (GHG) emissions. Emission scenarios produced by the Intergovernmental Panel on Climate Change (IPCC) accommodate for this by introducing so-called negative emissions. The underpinning logic of these scenarios is that the emissions budgets will be temporarily exceeded, to be compensated by massive amounts of negative emissions during the latter part of the century by removing the surplus of carbon dioxide from the atmosphere. The estimated budget for having a 66% chance of meeting the 1.5 °C target is 420 Gt starting from January 2018 [2]. With present emissions of around 42 Gt/year the budget would be exhausted already in 2028 and all emissions thereafter would need to be removed by negative emissions to meet the target.

The basic reactions for chemical-looping combustion of solid fuels can be described as follows [3,4].

$$\text{Solid fuel} \rightarrow \text{Volatile matter} + \text{Char} \quad \text{(R1)}$$

$$CH_4 + 4M_xO_y \rightarrow 4M_xO_{y-1} + CO_2 + 2H_2O \quad \text{(R2)}$$

$$C + H_2O \rightarrow H_2 + CO \quad \text{(R3)}$$

$$C + CO_2 \rightarrow 2CO \quad \text{(R4)}$$

$$CO + M_xO_y \rightarrow M_xO_{y-1} + CO_2 \quad \text{(R5)}$$

$$H_2 + M_xO_y \rightarrow M_xO_{y-1} + H_2O \quad \text{(R6)}$$

$$2M_xO_{y-1} + O_2 \rightarrow 2M_xO_y \quad \text{(R7)}$$

* Corresponding author.
E-mail address: xiaoyun.li@chalmers.se (X. Li).

https://doi.org/10.1016/j.fuproc.2021.106898
Received 5 January 2021; Received in revised form 9 May 2021; Accepted 14 May 2021
Available online 25 May 2021

When solid fuels are injected into a fuel reactor at high temperature, the solid fuels dry rapidly. After this the devolatilization (R1) of solid fuels takes place, typically within 1 s at 970 °C to generate char and volatiles [3]. Subsequently, the volatiles, containing CO, H_2 and hydrocarbons, will react directly with the oxygen carrier, e.g. R2, R5 and R6. The gasification (R3 and R4) of the char might take several minutes to generate H_2 and CO which can react with oxygen carriers directly (R5 and R6). Then the reduced oxygen carriers in fuel reactor will be transferred to the air reactor and oxidized by the air (R7). Finally, the oxidized oxygen carriers can be looped back to the fuel reactor to react with the fuels.

Ideally, pure CO_2 is obtained from the flue gas after condensation of the steam, resulting in inherent CO_2 separation. In reality, combustion of volatiles and char in the fuel reactor is incomplete. Unburnt char may be transferred to the air reactor together with oxygen carriers and unconverted volatiles can be observed at the outlet of the fuel reactor. A carbon stripper has been proposed and optimized to separate the unburned char from the oxygen carriers in order to improve the carbon capture efficiency of the whole process. Kramp et al. investigated the performance of a carbon stripper by simulations, which can improve the carbon capture efficiency of CLC of solid fuels from below 50% to more than 90% [5]. Sun et al. investigated the performance and operations of different carbon strippers experimentally, which gives a base for the carbon stripper application [6,7]. Different designs on carbon strippers have been demonstrated in different scales of CLC unit [8–10]. Important for reaching high CO_2 capture is sufficient fuel reactor temperature and use of small fuel particle size. Pilot operation with biomass has demonstrated it is possible to reduce the loss of carbon to the air reactor to less than 1–2% [11].

However, unreacted gases emitted from the fuel reactor together with CO_2 are also critical for the performance of CLC especially for solid fuels containing a large amount of volatiles. Unconverted gases can be addressed by addition of pure oxygen at the outlet of fuel reactor, which is called oxygen polishing [12]. But the presence of unconverted gases should be minimized to reduce the cost of oxygen production [13].

As a key for CLC, oxygen carriers for solid fuels are developed to low-cost and high-reactivity in recent years, i.e. ilmenite, iron ores, manganese ores or synthesized oxygen carriers [14–19]. Chemical-looping with oxygen uncoupling (CLOU) is a method proposed for improved or even full gas conversion in fuel reactor, since CLOU oxygen carriers can release gaseous oxygen, which can react with solid, liquid and gaseous fuels [20]. Mattisson et al. [20] and Leion et al. [21] showed that the conversion rate of solid fuels can be improved significantly by CLOU compared to conventional CLC. Various kinds of CuO-based, Mn-based and perovskite-type oxygen carriers synthesized with different supported materials by different techniques were studied, which showed high O_2-uncoupling capacity, sufficient reactivity and mechanical strength [22–28]. Different drawbacks of the above-mentioned CLOU oxygen carriers, such as the susceptibility to sintering and agglomeration, limited mechanical strength, slow oxidation kinetics and the deactivation due to impurities in the fuel [29–33], and production costs may potentially make CLOU materials less attractive for large-scale implementation.

Linderholm, et al., [3] investigated the CLC of solid fuels with different volatiles contents in 10 kW unit, and found a much lower gas conversion rate of solid fuels with higher volatiles content, which indicates that the volatiles released from the solid fuel have insufficient contact with the oxygen carriers in the fuel reactor. Abad, et al. found that feeding fuel into the carbon stripper and using the fuel reactor as a secondary reactor in a 50 kW_{th} CLC unit can improve the volatiles conversion and reduce the oxygen demand significantly [34]. A comparison of different fuel feeding positions, above-bed and in-bed, showed that in-bed fuel feeding method can increase the contact between the volatiles and the oxygen carriers which significantly improves gas conversion [3]. Similarly the gas conversion in a 100 kW unit using low-volatile fuel was high [9].

One reason for the lower gas conversion in fuel reactors for high-volatile fuels is the poor contact between volatile components and the oxygen carriers. The segregation of volatile components and higher-volatile particles was investigated under incipient bubbling conditions by different techniques [35,36]. The uprise of endogenous volatiles bubbles may reduce the contact between the volatiles and bed materials. Petersen and Werther modelled a circulating fluidized-bed gasifier for sewage sludge, which has high volatiles content, and found that plumes with high pyrolysis gas concentrations was formed in the vicinity of fuel feeding port and lateral mixing of the gas was not complete [37].

Going from small pilots to large-scale will greatly increase the cross-section area of fluidized-beds, and the volatiles can be expected to form a local plume over the fuel entry, with the consequence of reduced contact between volatiles and the bed material, i.e. the oxygen carrier in the case of chemical-looping combustion. There is thus a need to develop an effective and efficient solution that can improve the contact between the volatiles and the oxygen carriers in order to reach a higher gas conversion. Internals, i.e. vertical or horizontal tubes, fitted in fluidized-beds reduce bubble size, increase the emulsion voidage, reduce the gulf circulation of solids and thereby increase the overall residence time of reactant gas in the bed [38]. Massimilla and Johnstone illustrated that a fluidized-bed with baffle grids had much higher gas conversion than the non-baffled fluidized-bed [39].

Fundamental for CLC is the contact between combustible gases and the bed material that oxidizes the gases. The common practice in fluidized-bed boilers is to feed the fuel above the dense bottom zone. In CLC, however, it is desired that gases from the fuel are released as far down in the bed as possible. Here this need for higher gas conversion in the fuel reactor is addressed with a volatiles distributor. The key point of this unit is to distribute the volatiles evenly over the cross-section of the fluidized-bed. This idea can also be applied to other fluidized-bed processes, which require better gas-bed material contact.

2. Theory and experimental method

2.1. The volatiles distributor concept

If a box with an opening downwards is immersed in a fluidized-bed, it is known that the inside of the box will be free of bed materials and the bed surface level will be at the bottom edge of the box. However, if holes are made in the sides of the box, the bed level inside the box will increase to the holes level and the fluidization gas can pass through the holes, as shown in Fig. 1. If a gas is injected into this box above the side holes level, it will pass through the holes creating a pressure drop over the

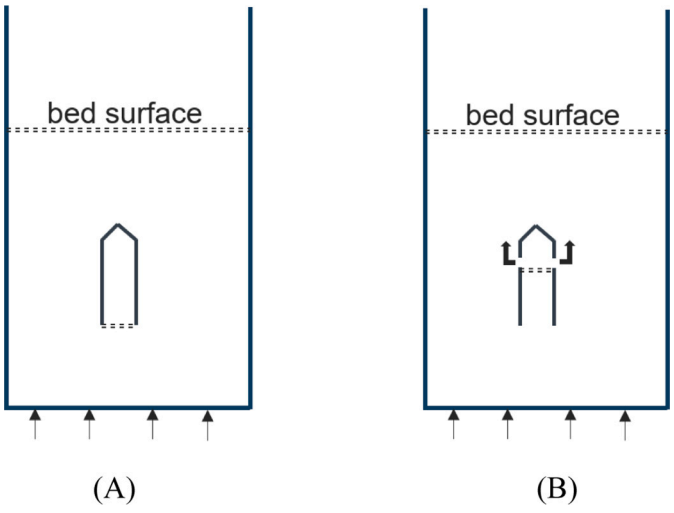

Fig. 1. Box immersed in a fluidized-bed. (A) without holes in the sides, (B) with holes in the sides.

holes. The increased pressure will lower the bed level inside the box.

Such a box can be extended to an arm and if a system of such arms is built and extended across the whole cross-section of a fluidized-bed, gases can be distributed via the holes in sides across the whole cross-section. Furthermore, this system can also be connected to the fuel feeding, in order to distribute the volatiles over the cross-section [13]. Fig. 2 shows how the fuel feed can be connected to the distributor arms. When the fine fuel drops down into the bed it is rapidly heated and releases its volatiles into the freeboard connected to the distributor arms.

The purpose of such a volatiles distributor is to avoid the situation with a local plume of volatiles over the location where the fuel is introduced in a fluidized-bed. Instead the volatiles distributor would allow for a good contact between the volatiles and the bed material, which is important to achieve good conversion in chemical-looping combustion. However, the principle can be also relevant for other purposes, like thermal gasification using dual fluidized-beds.

In this study, the concept of a volatiles distributor has been investigated in a cold-flow model. Thus, a distributor arm has been inserted in a 2D fluidized-bed, Fig. 3. Gases injected into the distributor arm can be used to simulate the volatiles released from solid fuels. In ideal cases, the inlet gas spreads over the length of the arm and is evenly distributed into the bed through the distribution holes. The gas flow through the holes is correlated with the pressure drop between the inside and outside the box at the holes level. The gas velocity through a grid hole can be calculated as follows [40].

$$v = C_d \sqrt{\frac{2\Delta P}{\rho_{gas}}} \tag{E1}$$

where ρ_{gas} (kg/m^3) is the gas density, ΔP (Pa) is the pressure drop between the inside and the outside the distributor at the holes level, that is $P_{in} - P_{out}$, and C_d is the orifice discharge coefficient.

The dense bed height inside the volatiles distributor can be estimated as follows.

$$h_b = \frac{P_{bottom} - P_{in}}{g^* \rho_{db,in}} \tag{E2}$$

where P_{bottom} (Pa) is the pressure at the lower edge of the VD, $\rho_{db,\,in}$(kg/m^3) is the solids density of the dense bed inside the VD, h_b (m) is the dense bed height inside the VD, g (m/s^2) is the gravitational acceleration.

Some typical orifice discharge coefficient values are shown in Table 1. The value of orifice discharge coefficient varies noticeably when the vessel Reynolds number is low. But a discharge coefficient 0.6 may be taken as standard when the Reynolds number is larger than 3000. The proper value of C_d could be affected by the presence of particles outside the holes as well as the pressure fluctuations typical of a fluidized-bed.

2.2. Experimental method

2.2.1. Cold-flow model

The experimental setup consists of a CFB cold-flow model shown in Fig. 4, the volatiles distributor, the gas supply system and the measurement system. The CFB model has a riser with a cross-section of 700 mm × 120 mm and a height of 8500 mm. The front plate of the riser is made from Perspex glass. Due to the large length/width ratio, the riser represents a two-dimensional geometry, which can be used to investigate the horizontal distribution of gases. There is an air distributor between the wind box and the riser, which is a perforated plate [41]. The position and the sketch of the volatiles distributor (VD) is shown in

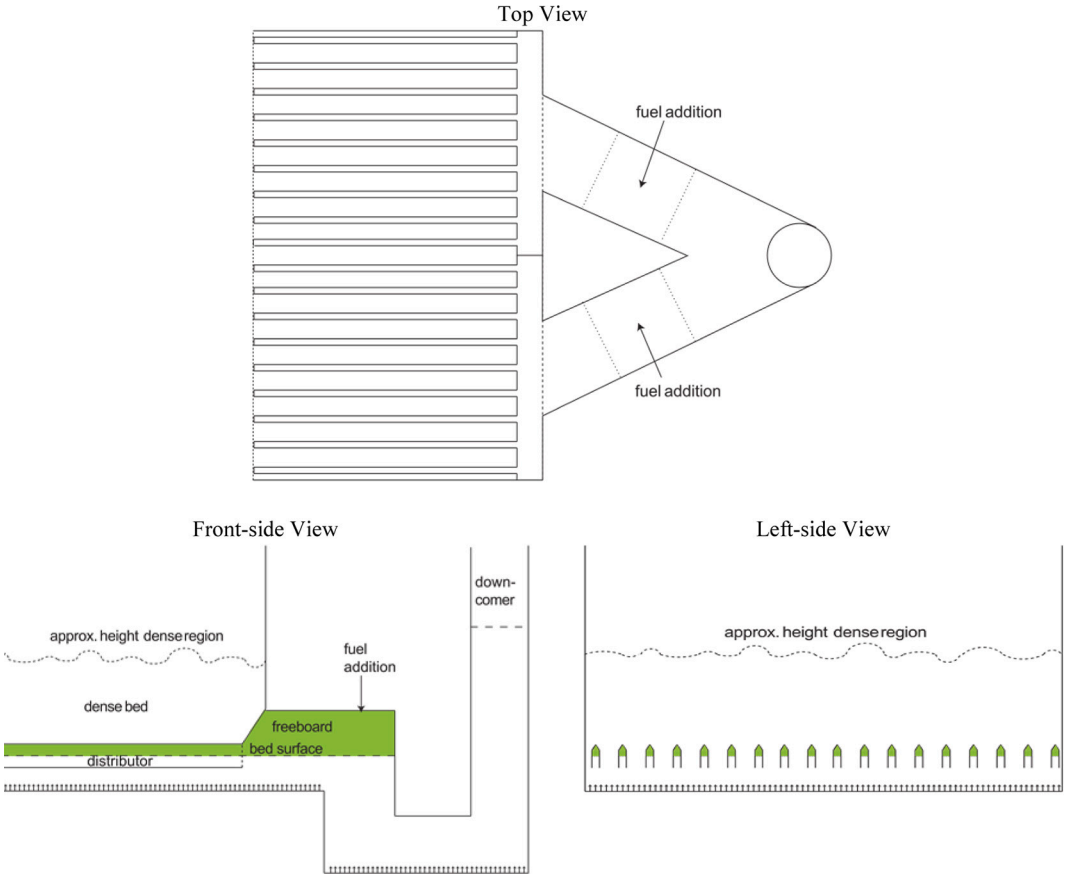

Fig. 2. Illustration of a volatiles distributor arrangement.

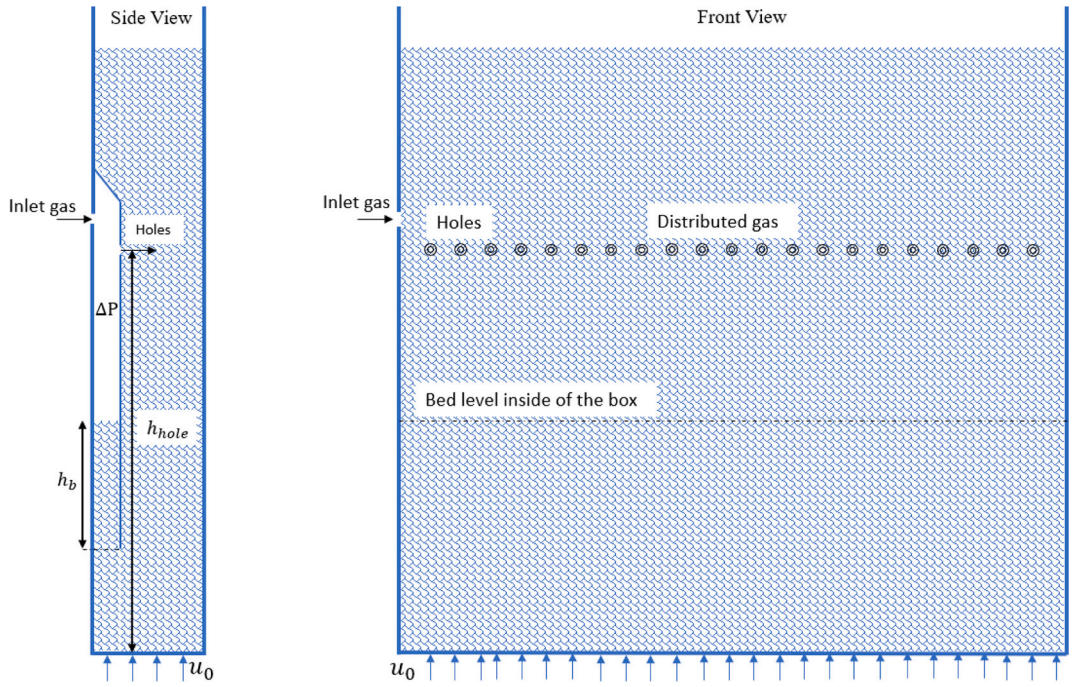

Fig. 3. Sketch of the half box and a 2D fluidized-bed.

Table 1
Some typical orifice discharge coefficient values for gas distributor.

Vessel Reynolds number, *Re*	100	300	500	1000	2000	>3000
Orifice coefficient, C_d	0.68	0.70	0.68	0.64	0.61	0.60

Fig. 4. The VD is attached on the front plate by bolts and nuts. There are 58 distribution holes in total with 5 mm diameter. Hence, the total area of these holes is 1.138×10^{-3} m^2. An injection pipe is attached on the front plate of the riser, where the simulated volatiles can be injected.

Two fans are used to supply primary air and air for the simulated volatiles. Pure CO_2 is used as tracer gas in the simulated volatiles gas stream. The flow rate of the tracer gas is controlled by a mass flow controller. The pure CO_2 and the air for the simulated volatiles are mixed and injected through the injection pipe attached on the front plate. The primary air is injected through the wind box at the bottom.

For the measurement system, there are 24 pressure taps in total in order to investigate the vertical pressure distribution along the riser height. 11 of these taps are densely spaced at the bottom first meter of the riser. There are two extra pressure taps added in order to measure the pressure drop between the inside and outside the VD at the level of the distribution holes. Piezo resistive pressure transducers are used for the pressure measurement. Most of the pressure transducers measure the vertical differential pressure between two pressure taps in order to achieve a high accuracy.

Two series of gas sampling tubes are installed at the back side of the bottom riser. The tubes reach 40 mm deep into the bed. The higher series consists of six sampling tubes, i.e. HSV1, HSV2, HSV3, HSV4, HSV5 and HSV6 shown in Fig. 4, evenly spaced at a height of 483 mm, and is used to measure the tracer gas. The horizontal distance of the sampling tubes from the left side of the riser is 124, 215, 306, 397, 480 and 579 mm respectively. Another series of gas sampling tubes, i.e. LSV1, LSV2, LSV3, LSV4, LSV5 and LSV6 shown in Fig. 4, is also located at the back side of the riser, but at a lower height, 138 mm. Thus, this series is located above the lower edge of the VD, with the intention to measure any gas leakage from the bottom of the VD. In each experiment, the CO_2 concentration in the simulated volatiles is adjusted to be close to 1%. The simulated volatiles distribution can be obtained by the measurement of CO_2 concentration at different horizontal positions and different heights. A gas analyzer, X-STREAM Enhanced XEGK, is used for the CO_2 concentration measurement of the gases sampled from the two series of sampling tubes. The gas sample flows continuously into the gas analyzer after filters at 1 L/min. The response time is 15 s. The concentration of CO_2 in air is around 400 ppmv [42]. Since CO_2 is used as tracer gas, all the CO_2 concentrations shown in the following sections are the added tracer gas CO_2 concentrations, i.e. the measured concentration minus the CO_2 concentration in ambient air during that specific experiment.

2.2.2. Bed material

The bed material used is silica sand with a density of 2600 kg/m^3 and a particle size range 250 μm–425 μm, both similar to those of bed materials in boilers. The particles are belong to group B in the Geldart classification, with a minimum fluidization velocity of 0.067 m/s and terminal velocity of 2.21 m/s at ambient conditions. 100 kg bed material is filled in the riser for each experiment.

2.2.3. Experimental conditions

Fluidization velocity is one of the most important parameters in the field of fluidization. Both bubbling fluidized-beds and circulating fluidized-beds are widely used in industry. Hence, the influence of fluidization velocity is investigated in this work. The fluidization velocity is calculated based on only the primary air flow, no matter how much simulated volatiles is injected into the VD. Two series of experiments with different operational conditions were conducted. The first series, which can be seen as the reference case includes the investigation of the simulated volatiles distribution at different fluidization velocities from 1 to 4 m/s without the VD. The second series investigates the performance of the VD at different fluidization velocities and different simulated volatiles flow rates. When the simulated volatiles flow varies, the primary air flow is kept. Thus, the difference between with and without VD can be analyzed. An overview of experimental conditions is shown in Table 2. Fluidization velocities were varied in a wide range. In a real application most of the gas in a fuel reactor comes from the fuel, whereas the fluidizing gas, e.g. steam, is kept low to reduce energy penalties associated with the fluidizing gas. The gases released from the

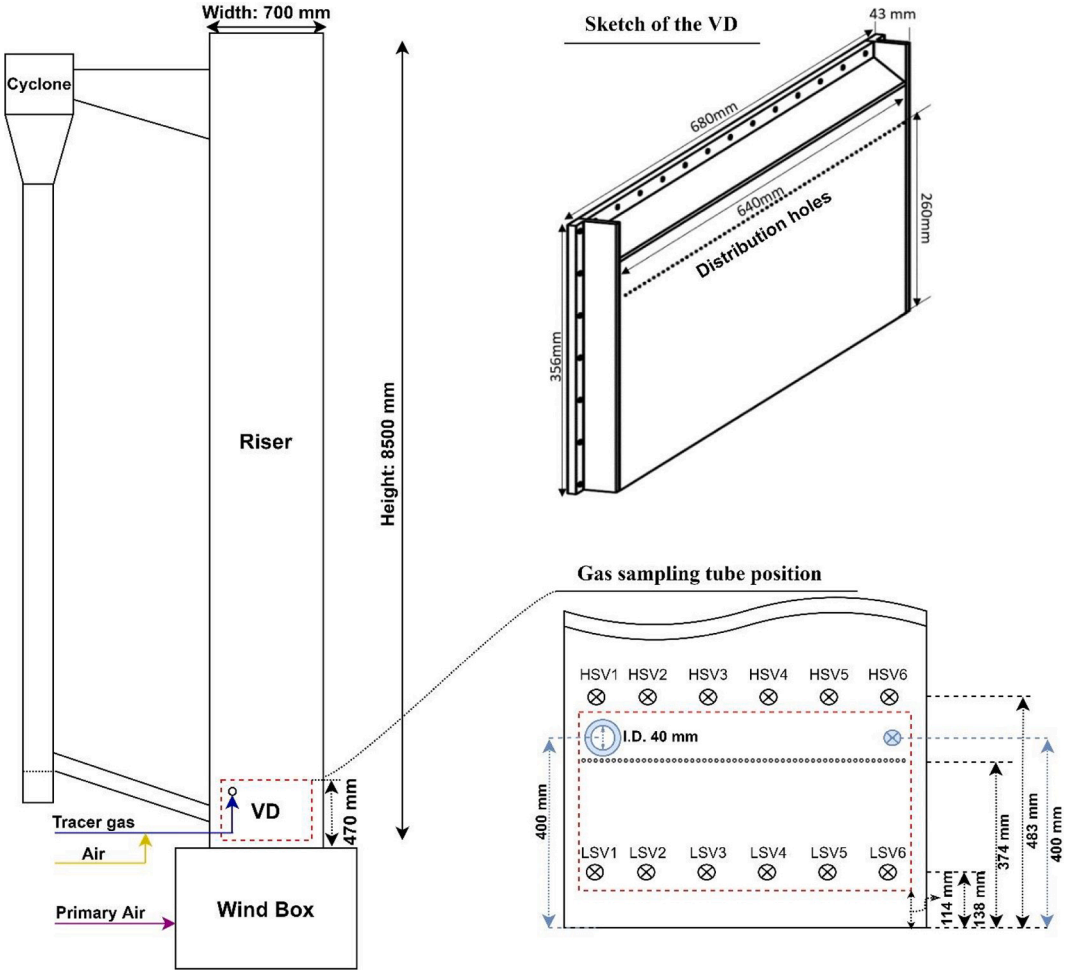

Fig. 4. Principal layout of the CFB cold-flow model and the sketch of the VD and gas sampling positions.

Table 2
An overview of the experimental conditions.

Test	u_0 (m/s)	CO_2 flow (L_n/min)	Air in SV (Nm^3/h)	VD	Bed material (kg)
1	1	5.6	19.5	Without	100
2	2	11.2	63.2		
3	3	16.8	93.5		
4	4	20.0	112.7		
5	1	5.6	18.4	With	
6		12.6	59.8		
7		20.0	100.7		
8	2	11.2	64.3		
9	3	16.8	91.5		
10	4	22.0	110.5		

Note: Air in SV – air flow in simulated volatiles.

gasification of the fuel will increase the fluidizing velocity, which means that the final fluidizing velocity will be significantly higher than the fluidizing velocity resulting from the fluidizing gas. For this reason it is motivated to study a range of fluidizing velocities.

Under each operational condition, the CO_2 concentration of gases sampled from the two series of sampling tubes is measured by the gas analyzer sequentially. First, the lower level of sampling tubes is measured starting from the position most distant from the CO_2 injection, i.e. LSV6, LSV5, LSV4, LSV3, LSV2, LSV1, cf. Fig. 4. After this, the higher level of sampling tubes is measured in the same sequence, i.e. HSV6, HSV5, HSV4, HSV3, HSV2, HSV1. The CO_2 concentration of each gas sampling tube was measured and recorded at 1 Hz during 120 s, with 90 s stabilization time before the data was recorded. When the data were analyzed, an averaged value was taken during the 120 s period. When the VD was present, one measurement was also made inside the VD on the right-hand side, i.e. the position shown in Fig. 4.

The pressure was measured at 50 Hz for each operational condition. A dense bed should be formed at the bottom of the riser, which can be characterized by a linear vertical pressure drop or constant solids concentration with height [43]. The dense bed height can be determined as the point where the pressure drop starts to deviate from the linear pressure drop.

3. Results

3.1. Experimental results in absence of the VD

Although the performance of the VD is the focus of this work, the typical solid density profile and the simulated volatiles distribution in absence of the VD were first investigated as reference cases. The reference cases were conducted at different fluidization velocities with the same bed material inventory.

Fig. 5 presents the vertical solids density profile obtained from the pressure drop measurements along the riser height in absence of VD. At the bottom of the riser, a dense bed region with constant solids density along height is formed, and higher fluidization velocity gives lower solids density. Above the dense bed region, a splash zone is formed with an exponential decay in solids density, caused by the strong back-mixing by means of ballistic movement of clustered particles. A transport zone with lower exponential decay above the splash zone occupies most of the

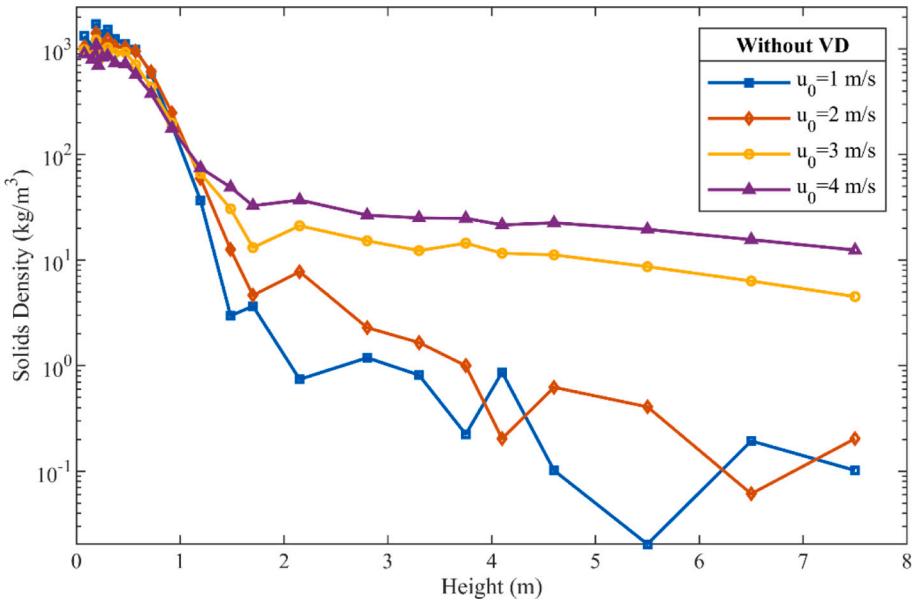

Fig. 5. Influence of the fluidization velocity on the vertical solids density profile, obtained from pressure drop measurements, in absence of VD.

riser height and has a dispersed solids flow with back-mixing mostly at the riser wall. Higher fluidization velocity transfers more bed materials from the bottom to the transport zone. Thus, the solids density in the transport zone is much higher at higher fluidization velocity. The solids density at lower fluidization velocities becomes more uncertain in the transport zone, because they are associated with measurements of small pressure drops.

Fig. 6 shows the CO_2 concentrations at different positions. The measurement sequence is LSV6, LSV5, LSV4, LSV3, LSV2, LSV1, HSV6, HSV5, HSV4, HSV3, HSV2, HSV1, cf. Fig. 4. The experimental data for each position were recorded for 120 s. There is essentially no CO_2 detected at the lower level except for LSV1, which is closest to the simulated volatiles injection. This minor CO_2 concentration at LSV1 is due to the fluctuations of fluidization. As expected the majority of the CO_2 is found in HSV1 and HSV2, close to the inlet of CO_2 gas injection (See Fig. 4).

3.2. Experimental data with VD

The variation in solids density from the bottom to the top of the riser in the presence of VD, Fig. 7, is generally similar to what is seen in absence of VD. Higher fluidization velocity gives higher solids density in the upper part of the riser. But the solids density at the bottom decreases slightly up to 300 mm height, and then increases up to 470 mm, which is exactly the top end of the VD. The presence of the VD gives a higher velocity locally, which explains the lower density in this height range.

Fig. 8 gives an overview of the tracer gas concentrations for 4 m/s. The measurements in the lower part show low tracer gas CO_2 concentration with the highest close to the simulated volatiles injection position. There maybe two sources of this CO_2. The first one is back mixing of the simulated volatiles from the distribution holes of the VD. Such back mixing was seen in the case of no VD, Fig. 6. The second one is leakage of the simulated volatiles from the bottom of the VD. At the higher level, HSV1 to HSV6, it is seen that the simulated volatiles are distributed

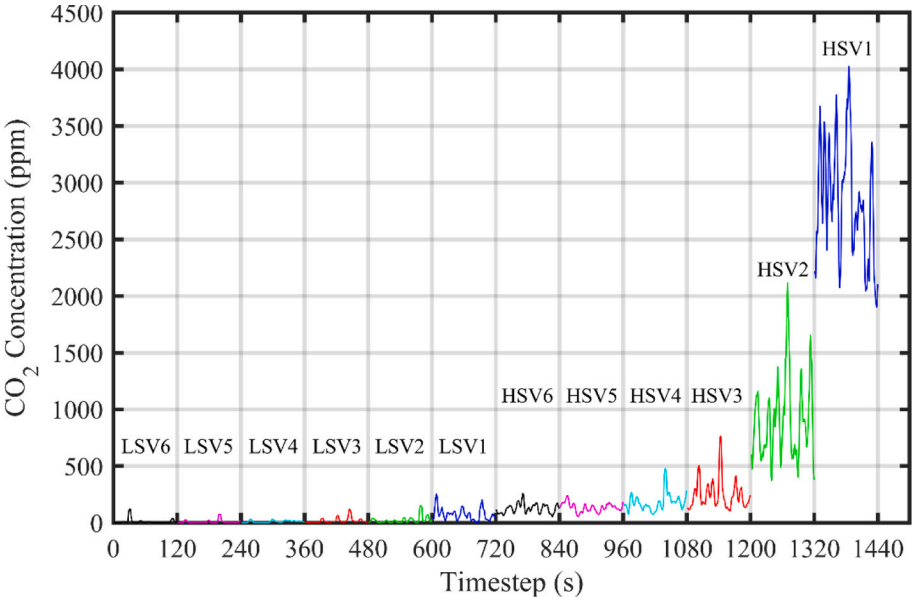

Fig. 6. CO_2 concentration signal at different measurement positions in absence of the VD (u_0 = 4 m/s).

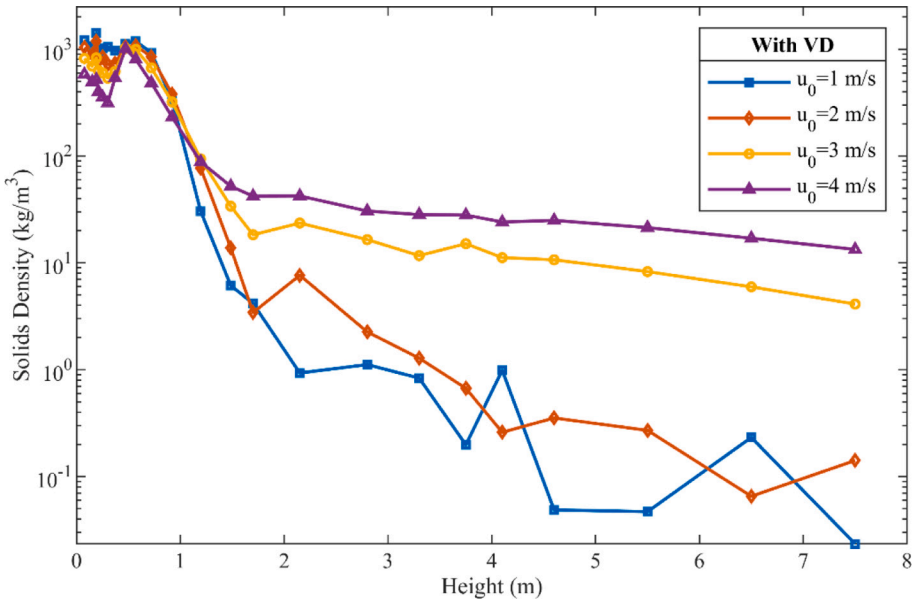

Fig. 7. Influence of the fluidization velocity on the vertical solids density profile, obtained from pressure drop measurements, in the presence of VD.

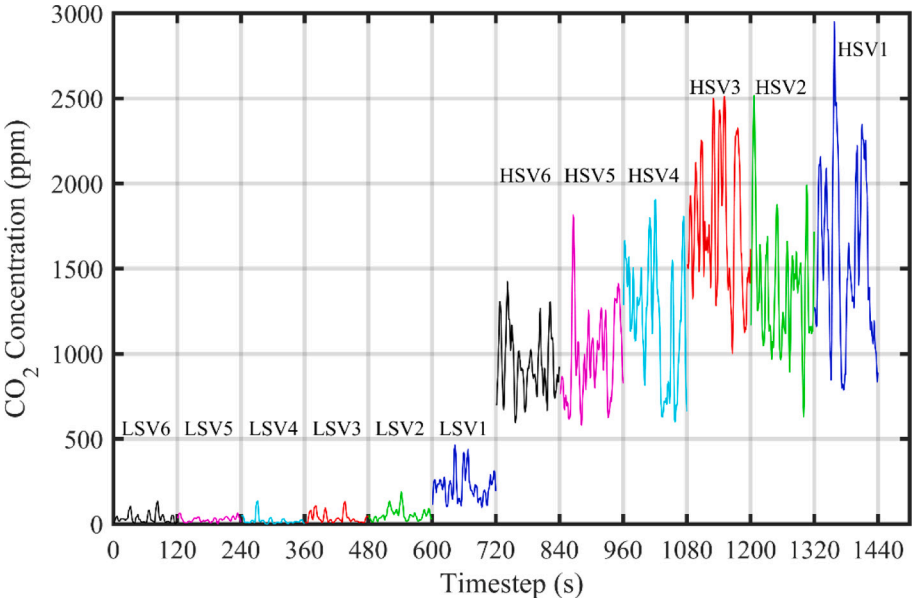

Fig. 8. CO_2 concentration signal at different measurement positions with the presence of the VD (u_0 = 4 m/s).

more evenly in the presence of VD, i.e. in comparison to the concentrations seen in Fig. 6.

3.3. Influence of the fluidization velocity on the performance of VD

To evaluate the simulated volatiles distribution along the length of the riser under different operational conditions with and without VD, a CO_2 ratio was defined as the ratio of the CO_2 concentration measured by the gas analyzer at different positions to the expected average CO_2 concentration in the riser cross-section, see Eq. (E3).

$$R = \frac{c_m}{c_{cal}} \tag{E3}$$

where c_m (ppm) is the average measured CO_2 concentration during 120 s by the gas analyzer and c_{cal} (ppm) is the calculated CO_2 concentration from the flow rates of primary air, air used to simulate volatiles and CO_2 injected as tracer gas.

Hence, the calculated CO_2 concentration can be obtained from Eq. (E4).

$$c_{cal} = \frac{MF_{CO_2}}{MF_{PA} + MF_{SA} + MF_{CO_2}} \tag{E4}$$

where MF_{CO2}, MF_{PA} and MF_{SA} are flow rates of CO_2 as tracer gas, primary air for the main fluidization and air flow for simulated volatiles.

Fig. 9 shows the CO_2 ratio from left to right, i.e. LSV and HSV positions 1 to 6, at different fluidization velocities in absence of VD. When the fluidization velocity increases, more volatiles will pass through the left side of the riser which is near the simulated volatiles injection side. Since higher fluidization velocity causes larger bubbles and higher bubble rising velocity, bubbles from the bottom distributor coalesce more easily with the bubbles formed by the simulated volatiles. Hence, a larger gas upflow above the simulated volatiles injection position is

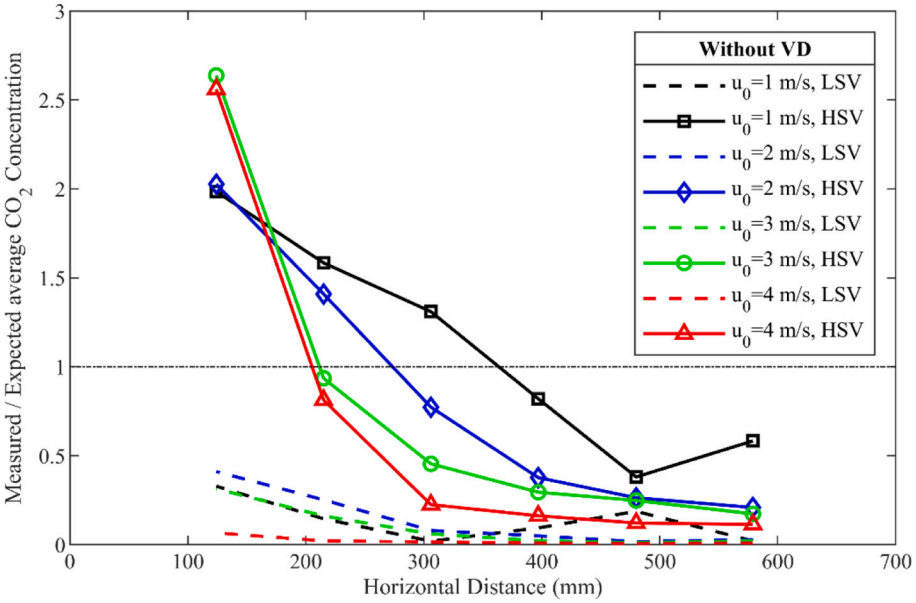

Fig. 9. Influence of fluidization velocity on the volatiles local plume formation in absence of VD.

formed at higher fluidization velocity, which leads to poorer horizontal volatiles dispersion and more pronounced volatiles segregation. Thus, a more local plume of volatiles is formed at higher fluidization velocity. Furthermore, higher fluidization velocity gives less CO_2 in the lower part, which means there is less back mixing.

Compared to the CO_2 ratios without VD, the ones with VD are closer to the expected average concentration, as shown in Fig. 10. Moreover, in presence of VD, the variation in CO_2 ratio decreases with the rising velocity. This is the opposite trend as compared to that found in the absence of VD in Fig. 9. With the VD, less volatiles were detected at the lower positions, especially at the left, which is near the location where volatiles are injected.

The CO_2 ratios at different positions of the higher level are analyzed further in order to evaluate the VD performance. The calculation results are presented in Table 3. The arithmetic mean value as a statistical indicator is used to describe the central tendency of a data set, Eq. (E5).

$$A(x_1, x_2, \ldots x_n) = \frac{\sum_{i=1}^{n} x_i}{n} \tag{E5}$$

Here, the average CO_2 ratio over the six horizontal measurement positions under the same fluidization velocity in the presence of VD is reasonably close to 1, which means the CO_2 measured at the six positions are representative or well-matched to the real CO_2 distribution at this level. However, the average CO_2 ratio decreases from near 1 to 0.67 with the increasing of fluidization velocity when there is no VD installed. With 0.04 m penetration, the gas suction tubes were situated half-way between the back wall and the wall of VD. In absence of VD the tubes only penetrate one third of the distance between the walls. It is not unlikely that concentrations are higher closer to the front wall where the simulated volatiles are injected, which may explain the lower average CO_2 ratio at higher velocities.

Another likely explanation for the lower average concentration in some measurements is related to the flow pattern in the bed. The bottom

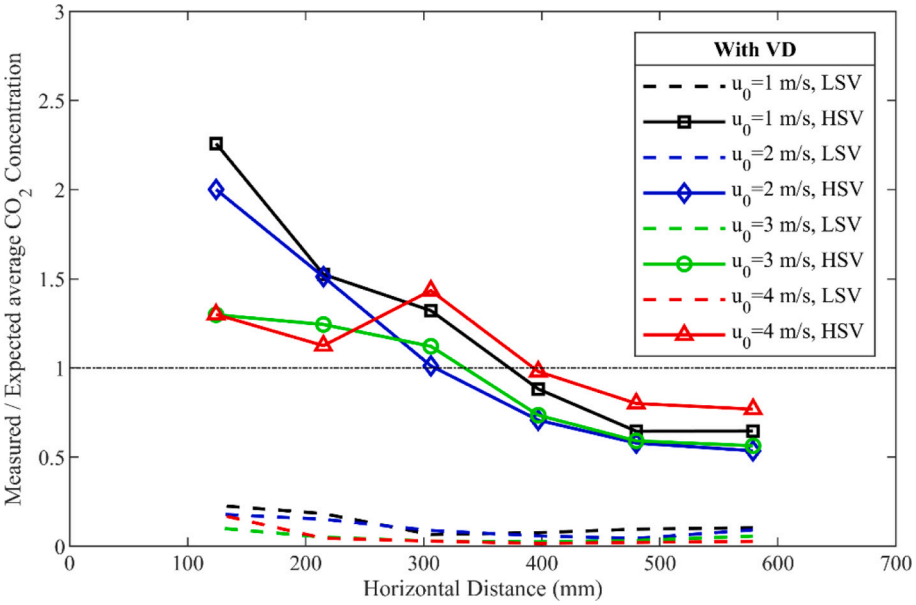

Fig. 10. Influence of fluidization velocity on the VD performance.

Table 3
Data analysis of VD performance at different fluidization velocities.

Fluidization velocity u_0, m/s	Average CO_2 ratio		Standard deviation		Relative standard deviation		Highest/lowest concentration	
	Without VD	With VD	Without VD	With VD	Without VD	With VD	Without VD	With VD
1	1.11	1.21	0.57	0.57	51%	47%	5.21	3.50
2	0.84	1.06	0.67	0.54	80%	51%	9.70	3.73
3	0.79	0.93	0.86	0.30	109%	32%	15.24	2.30
4	0.67	1.07	0.88	0.24	131%	22%	22.50	1.86

bed of a circulating fluidized-bed operates in the "exploding bubble" regime [41], where a significant part of the gas by-passes the bed as through flow or bypass flow [43]. This through flow of gas is assumed to be made up of bubble chains or channels creating short circuits of gas bypassing the bottom bed. This gas moves with a much higher velocity and any component of this gas will be underrepresented by a suction probe which measures the local average concentration. Likewise, would the simulated volatiles be underrepresented if they would be sucked into this flow. The fraction of through flow also increases with increasing fluidization velocity, which is also consistent with the results without VD.

The standard deviation of CO_2 ratio at the six measurement positions is calculated as well in order to evaluate how evenly the volatiles are distributed, Eq. (E6). Again, it can be seen that the distribution is more even with the volatiles distributor, in particular at higher velocities, Table 3.

$$\sigma = \sqrt{\frac{\sum_{n=1}^{N}(x(n) - A)^2}{N-1}} \tag{E6}$$

where N is the total number of data points, A is the average value and $n = 1, 2, 3, \ldots, N$.

Relative standard deviation (RSD) gives a variation range of the majority in a number set, Eq. (E7). What Table 3 tells is that the variation range is larger with the rising fluidization velocity in absence of VD. But it gets quite narrower with VD, especially at higher fluidization velocities.

$$RSD = \frac{\sigma}{A} \times 100\% \tag{E7}$$

The highest concentration divided by the lowest one at the six measurement positions under different operation conditions were shown as highest/lowest concentration in Table 3. Also this ratio indicates a more even distribution in presence of the VD.

3.4. Influence of the simulated volatiles flow rate on the VD performance

The performance of VD was investigated with different simulated volatiles flow rates under the same overall fluidization velocity. The flow rate of simulated volatiles was varied in order to simulate the variation of fuel feeding rate.

As Table 4 shows, when the flow rate of simulated volatiles increases, the pressure inside the VD increases about 0.9 kPa. But the pressure outside VD measured at the back side of the riser at the holes level, doesn't increase that much, about 0.15 kPa. Thus the pressure drop between inside and outside VD increases with the increase of simulated volatiles flow rate.

Fig. 11 shows the influence of increasing volatiles flow rate on the volatiles distribution at higher and lower level. When the volatiles flow rate increases, more volatiles can be found at the lower level, at least to the left. It is hard to verify where the increased concentration of volatiles comes, either from leakage below the bottom of the VD due to the pressure fluctuations inside the VD, or back mixing outside the VD. But increased leakage is more likely considering the higher pressure inside the VD pressing down the bed level, whereas there is no obvious reason why back-mixing outside the VD should increase significantly. At the higher level, the effect of increased volatiles flow on the CO_2 ratio is small, although the highest flow shows somewhat improved distribution.

Table 4
Pressures under different flow rates of simulated volatiles.

Fluidization velocity u_0, m/s	1		
Simulated volatiles flow rate V_{sv}, Nm^3/h	19	61	102
Pressure inside the VD P_{in}, kPa	6.50	7.08	7.38
Pressure outside VD at holes level P_{out}, kPa	5.38	5.53	5.52
Pressure drop between inside and outside VD ΔP, kPa	1.12	1.55	1.87

An evaluation on VD performance at different simulated volatiles flows is presented in Table 5. The average CO_2 decreases from 1.21 to 1.01 with increasing of simulated volatiles flow, but there is no clear trend for the standard deviation, relative standard deviation or highest/lowest concentration. Even though the volatiles flow is increased five times, the changes are moderate.

3.5. Volatiles concentration inside the VD

To achieve a good distribution, the volatiles concentration in VD should show low variation. In order to investigate the volatiles concentration inside the VD, the CO_2 concentration at the top right corner of VD was measured as shown in Fig. 12. There is no significant CO_2 measured in the absence of VD as expected. When the fluidization velocity increases, the simulated volatiles flow was designed to be increased correspondingly in this series of experiments. It can be seen that CO_2 concentration in the top right corner of VD increases with the rising fluidization velocity. When the fluidization velocity is fixed at 1 m/s, CO_2 concentration to the top right corner of VD increases with rising flow of simulated volatiles as shown in Fig. 13.

Even though the target CO_2 concentration in the simulated volatiles was 10,000 ppm, there were significant deviation in some cases. Hence, the ratio of CO_2 concentration at the right corner of the VD to the CO_2 concentration in the incoming simulated volatiles, i.e. c_{VD}/c_{sv}, is analyzed to investigate the dilution inside the VD. Table 6 indicates that significant dilution of the simulated volatiles takes place inside the VD, in particular at low velocities. The dilution should be highest at this point which is most far away from the inlet of simulated volatiles. Nevertheless, the dilution indicates that there is a significant gas flow with visual observation of the fluidization inside the VD.

4. Discussion

4.1. Solids density

Fig. 14 illustrates the solids density difference at the bottom of the riser caused by the installation of VD. The solids density is lower in the presence of VD compared to that without VD from the bottom up to 470 mm height. Since the width of VD is 43 mm, and it occupies one third of the total width of the riser, more fluidization air passes through the remaining two thirds of the riser which gives a higher air velocity and makes the bed material more dilute in the bottom part. The difference increases with increasing overall velocity. However, this effect is expected to be less pronounced in a real-world application, where the distributor arms would cover a smaller fraction of the cross-section.

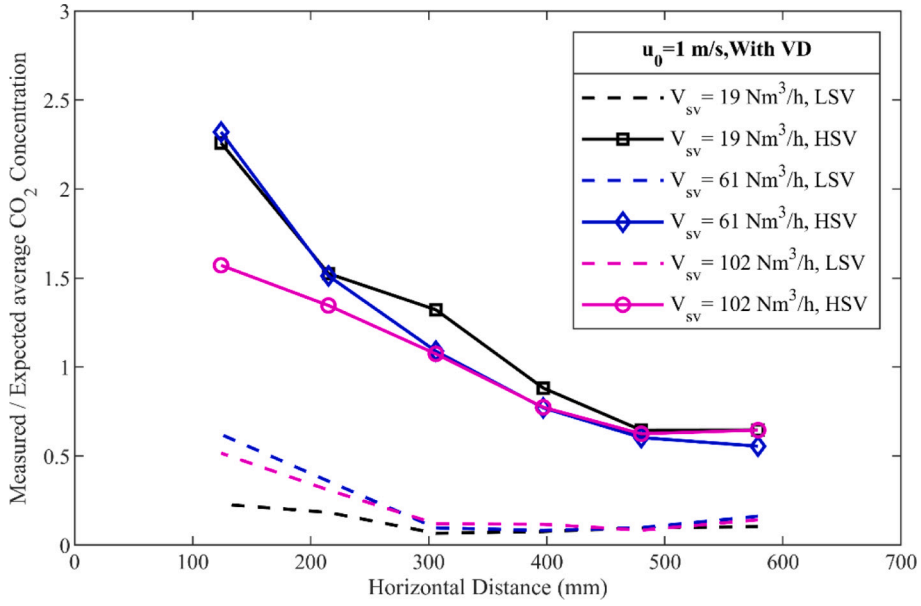

Fig. 11. Influence of simulated volatiles flow rate on the VD performance.

Table 5
Data analysis of VD performance at different simulated volatiles flow rates.

Fluidization velocity	Simulated volatiles flow rate	Average CO_2 ratio	Standard deviation	Relative standard deviation	Highest/lowest concentration
u_0, m/s	V_{sv}, Nm^3/h				
1	19	1.21	0.57	47%	3.50
	61	1.14	0.62	54%	4.18
	102	1.01	0.36	36%	2.51

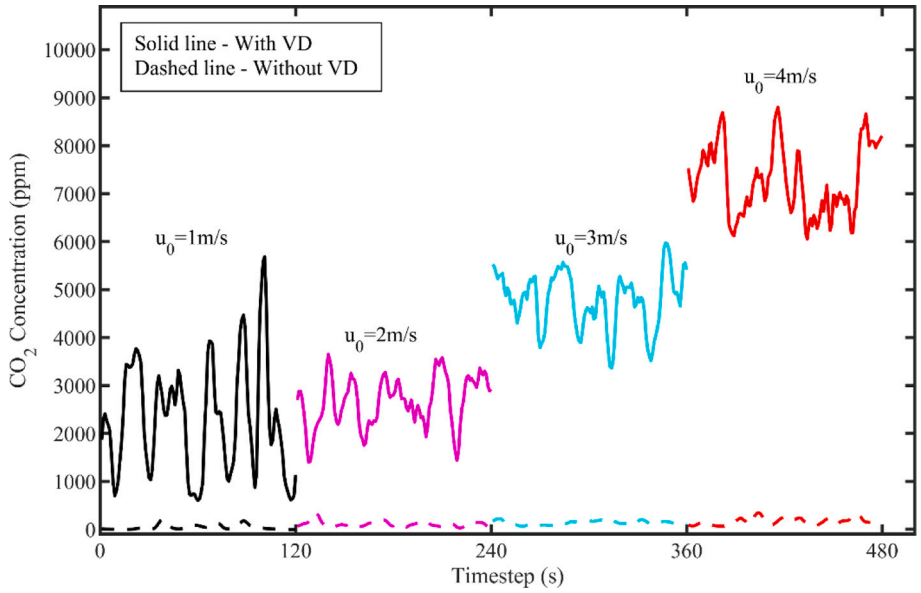

Fig. 12. CO_2 concentration signal measured from at the top right corner inside the VD at different fluidization velocities.

4.2. Pressure fluctuations

Analysis of pressure fluctuation in fluidized-bed can be used to characterize flow behaviors. When the bed is fully fluidized, the time-average pressure at a specific level approximately matches the weight of the bed materials above the level. Amplitude of pressure fluctuations, as standard deviation, is generally and closely related to the size and behavior of bubbles in the fluidized-bed [44]. Table 7 presents the data analysis results about the pressure fluctuations inside and outside VD. As the fluidization velocity increases, the pressure inside and outside VD at the holes level increases, because of more bed materials transported to the upper part of the riser. The amplitude of the pressure outside VD at the level of the holes increases both with raised fluidization velocity and raised simulated volatiles flow. The amplitude of pressure fluctuations

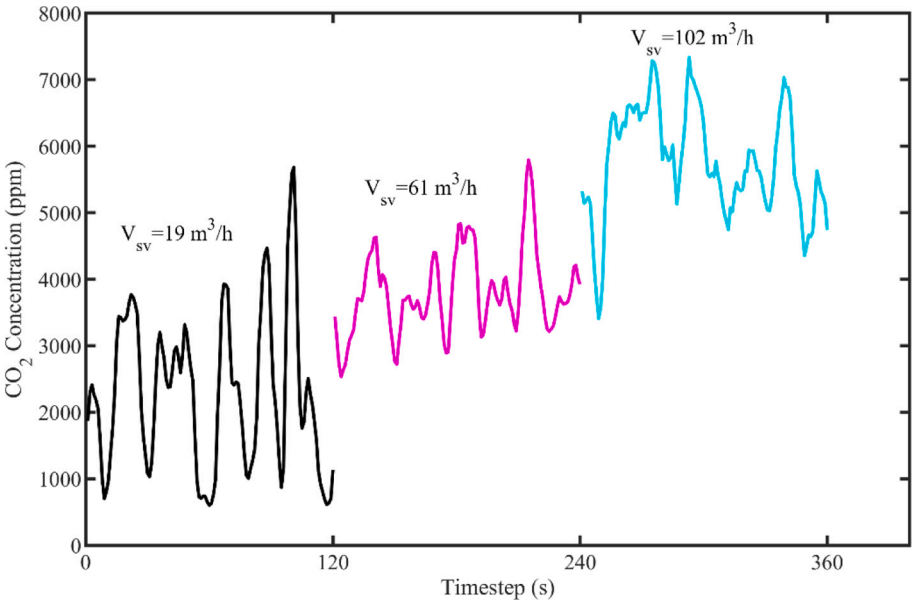

Fig. 13. CO_2 concentration signal measured from at the top right corner inside the VD at different simulated volatiles mass flow rates. (u_0 = 1 *m/s*).

Table 6
Volatiles dilution inside the VD.

u_0	CO_2 flow	Air to SV	c_{sv}	c_{vd}	c_{vd}/c_{sv}
m/s	(L_n/min)	(Nm^3/h)	(ppm)	(ppm)	
1	5.6	18.4	17,933	2767	0.15
	12.6	59.8	12,484	4307	0.34
	20.0	100.7	11,776	6307	0.54
2	11.2	64.3	10,343	3146	0.30
3	16.8	91.5	10,896	5269	0.48
4	22.0	110.5	11,805	7718	0.65

Note: Air to SV – air flow injected to simulated volatiles; c_{sv} – CO_2 concentration in the simulated volatiles; c_{vd} – CO_2 concentration measured to the top right corner of VD.

Table 7
Analysis of pressure fluctuations inside and outside the VD.

Fluidization velocity u_0, m/s	1			2	3	4
Simulated volatiles flow rate V_{sv}, Nm^3/h	19	61	102	65	92	112
Average pressure outside VD P_{out}, kPa	5.38	5.53	5.52	5.54	5.76	6.39
Standard deviation of pressure outside VD σ_{out}, Pa	58.5	71.5	74.7	61.4	94.6	148.9
Average pressure inside VD P_{in}, kPa	6.50	7.08	7.38	7.32	7.34	7.56
Standard deviation of pressure inside VD σ_{in}, Pa	98.1	91.9	85.5	57.7	83.9	171.3

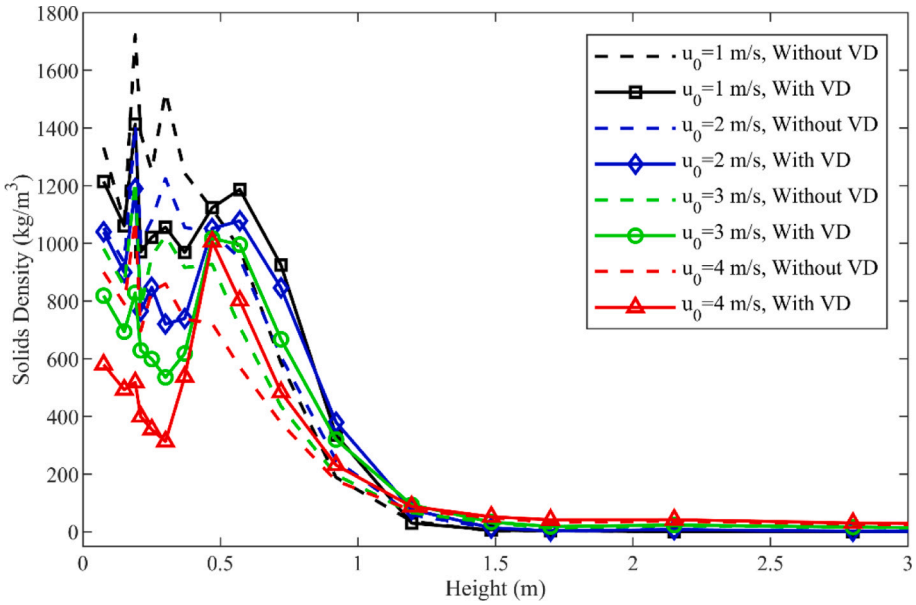

Fig. 14. Solids Density Difference between with and without VD.

inside VD generally increases, as the fluidization velocity increases from 2 to 4 m/s. On the other hand it falls when only the simulated volatiles mass flow rate changes.

4.3. Bed level inside the VD

Since the pressure taps are densely spaced at the bottom of the riser and there is a linear vertical pressure drop at the bottom dense bed, the bed level inside the VD can be estimated based on the time-average pressures inside and bottom of the VD. The bed level inside the VD is given by Eq. (E2), and the results are shown in Table 8. The decrease in pressure drop inside the VD is linked to a decrease in solids inventory inside VD. To estimate the bed height inside the VD, the solids density is assumed to be the same as the one at 1 m/s.

When the fluidization velocity is 4 m/s, the estimated pressure at the bottom of VD is slightly lower than that inside VD, which is not reasonable and is likely explained by an inaccuracy of the measurement. However, the trends are reasonable. When the volatiles flow and fluidization velocity are increased, the bed surface inside the VD is lowered. There are two effects. Firstly the increased volatiles flow should give more pressure drop over the holes, which increases the pressure, thus pressing down the bed level. Secondly, increased fluidization velocity gives lower pressure drop outside the VD, cf. Fig. 14, which is compensated by lower pressure drop inside the VD, i.e. lower bed height.

4.4. Dilution of volatiles inside the VD

When the volatiles are injected into VD, it will be diluted by the air from the main fluidization. According to the results in Section 3.5, more volatiles injected and higher fluidization velocity give less volatiles dilution. The flow of fluidization air from the bottom of the VD causing dilution of volatiles inside the VD is estimated below.

The pressure drop between inside and outside VD at the holes level, i.e. ΔP, is known. Then Eq. (E1) can be used to calculate the gas velocity through the orifices of VD. The orifice coefficient, C_d is assumed to be 0.6 in accordance with the vessel Reynolds number estimation in Table 1 [40]. Since more than 99.5% of the gas used in this series of experiments is air, the density of gas is assumed to be equal to the density of air, ρ_{air}. The orifices area, $A_{orifice}$, is already known. Thus the total gas flow through the orifices of VD, i.e. $V_{orifice}$, can be calculated as Eq. (E8). Since the flow of simulated volatiles injected to VD, V_{sv} is known, the remaining gas going upwards inside the VD from the bottom, V_{ba} can be obtained based on Eq. (E9). Furthermore, the total flow going inside VD, $V_{orifice}$, and the total CO_2 flow injected to VD, V_{CO2}, are known, then the average CO_2 concentration inside VD can be calculated as Eq. (E10), which can be compared to the CO_2 concentration measured at the right top corner of VD, i.e. c_{vd}. The average concentration inside the VD is expected to be higher than that measured in the right corner far from the inlet.

$$V_{orifice} = v_{orifice} \times A_{orifice} \tag{E8}$$

$$V_{ba} = V_{orifice} - V_{sv} \tag{E9}$$

Table 8
Bed level inside the VD calculated from pressure at VD bottom edge.

Fluidization velocity u_o, m/s	1			2	3	4
Simulated volatiles flow rate V_{sv}, Nm^3/h	19	61	102	65	92	112
Average pressure inside VD P_{in}, kPa	6.50	7.08	7.38	7.32	7.32	7.56
Average pressure at the bottom of VD P_{bottom}, kPa	8.16	8.24	8.16	7.74	7.38	7.51
-dP/dH, kPa/m	10.52					
Bed level inside VD h_b, m	0.16	0.11	0.07	0.04	0.01	–

$$c_{vd,cal} = V_{CO_2} / V_{orifice} \tag{E10}$$

According to the calculation results shown in Table 9, less air will go inside the VD from the bottom, when the simulated volatiles flow and overall fluidization velocity are raised. In the later case, this is most likely explained by the fact that the simulated volatiles flow is also increased when the fluidization velocity is raised.

Another way to estimate the flow coming into the VD from below is to assume that the CO_2 concentration distribution outside VD are proportional to that inside. This includes the assumption that the CO_2 concentration measured at position of HSV6 corresponds to the one measured at the right top corner inside the VD. Then the average CO_2 ratio of the six higher level positions divided by the one at HSV6, i.e. Average/HSV6, should correspond to the average CO_2 concentration inside VD divided by the CO_2 concentration measured at the right top corner of VD, i.e. $c_{vd,\ cal}'/c_{vd}$. With this relationship, i.e. Eq. (E11), the average CO_2 concentration in the VD at each operational condition can be estimated. Furthermore, since the CO_2 flow injected to VD is known, the total flow passing through the VD can be calculated based on Eq. (E10). Based on total flow passing through the VD and the simulated volatiles flow injected into the VD, the air coming into the VD from below can be estimated by Eq. (E9). The results are shown in Table 10. Similar trends were obtained from this second estimation method. The air coming into the VD from below falls with rising volatiles flow and fluidization velocity, except for a slight increase from 1 m/s to 2 m/s.

$$\frac{\text{Average}}{\text{HSV6}} = \frac{c_{vd,cal}'}{c_{vd}} \tag{E11}$$

From the estimated bottom air flow going upwards inside the VD, the fluidization velocity inside the VD can be calculated, see Fig. 15, where the two methods to estimate the flow are compared. The results from two methods are in the same order of magnitude, and show the same trend, i.e. decreasing flow and velocity with increased volatiles flow.

5. Conclusion

This initial experimental study performed in a circulating fluidized-bed cold-flow model validates the effectiveness of a volatiles distributor. When there is no VD, the simulated volatiles form a local plume which is more pronounced at higher fluidization velocities. The presence of the VD significantly contributes to a more uniform horizontal distribution of volatiles. The horizontal distribution without and with VD was measured at six lateral positions, and the relative standard deviation decreases from 131% to 22% at the higher fluidization velocity. Similarly, the ratio of highest to the lowest CO_2 concentration decreases from 22.5 to 1.86. Hence, the positive effect of the VD on the lateral distribution of the volatiles is enhanced at higher velocities. For chemical-looping combustion of solid fuels, two interconnected circulating fluidized-beds are usually used for air and fuel reactors, both expected to have higher fluidization velocity in commercial scale. The VD could be an important tool to achieve good contact between volatiles and bed materials in the fuel reactor.

Increased volatiles flow, when keeping the fluidization velocity constant, has no obvious influence on the horizontal distribution, but increases the pressure drop between inside and outside the VD from 1.12 to 1.87 kPa, which consequently lowers the bed level inside the VD and decreases the flow of fluidization air from the bottom of the VD.

In the case where both the fluidization velocity in the main riser and volatiles flow increase proportionally, the outside pressure drop along the height of the VD, i.e. the solids density, falls, while the pressure drop between inside and outside the VD decreases from 1.78 to 1.17 kPa and less fluidizing gas goes into the VD.

The measurements at the lower-level sampling positions, show slightly higher concentration of volatiles at the left side, i.e. in LSV1 position, because of back mixing mostly. The measured/expected

Table 9
Bottom fluidization air mixed with simulated volatiles in VD.

u_0	ΔP	C_d	ρ_{air}	$v_{orifice}$	$A_{orifice}$	$V_{orifice}$	V_{sv}	V_{ba}	V_{CO_2}	$c_{vd,\ cal}$	c_{vd}
m/s	Pa	–	kg/m^3	m/s	m^2	Nm^3/h	Nm^3/h	Nm^3/h	Nm^3/h	ppm	ppm
1	1115	0.6	1.189	26	1.138×10^{-3}	106	19	87	0.34	3151	2302
	1548			31		125	61	64	0.76	6027	3813
	1869			34		138	102	36	1.20	8705	5763
2	1776			33		134	65	69	0.67	4999	2667
3	1612			31		128	92	36	1.01	7870	4796
4	1204			27		111	112	−1	1.32	11,933	7270

Table 10
Volatiles dilution estimated according to the proportional volatiles distribution inside and outside VD.

u_0	CO_2 ratio		Average/HSV6	c_{vdu}	$c_{vdu,\ cal}'$	V_{CO2}	$V_{orifice}$	V_{sv}	V_{ba}
m/s	HSV6	Average		ppm	ppm	Nm^3/h	Nm^3/h	Nm^3/h	Nm^3/h
1	0.6460	1.21	1.88	2302	4323	0.34	78	19	59
	0.5554	1.14	2.06	3813	7840	0.76	96	61	35
	0.6455	1.01	1.56	5763	8981	1.20	134	102	32
2	0.5360	1.06	1.97	2667	5263	0.67	128	65	63
3	0.5637	0.93	1.64	4796	7875	1.01	128	92	36
4	0.7690	1.07	1.39	7270	10,099	1.32	131	112	19

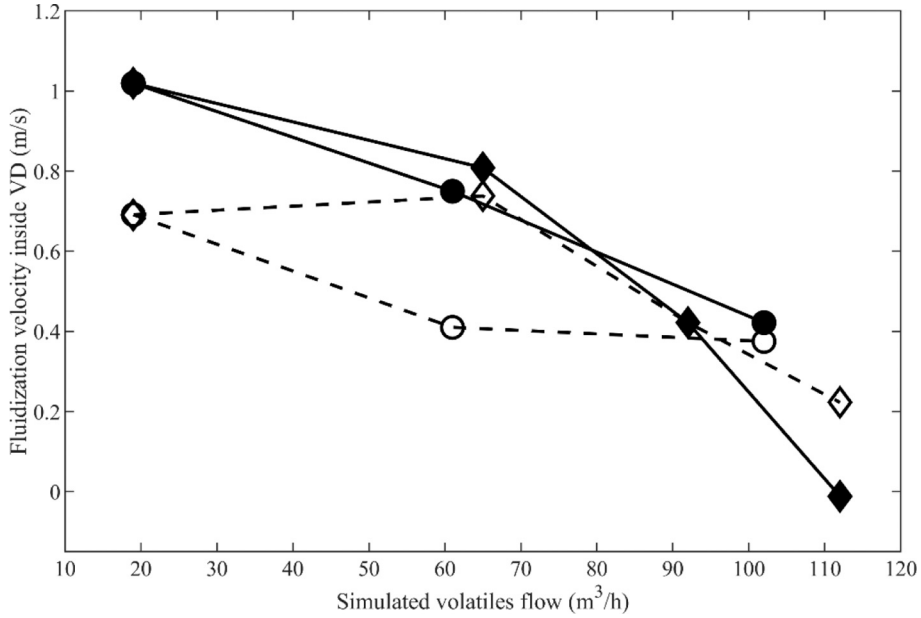

Fig. 15. Fluidization velocity inside VD as a function of simulated volatiles flow. Solid lines use data from Table 9 and dashed lines data from Table 10. Circles denote varied volatiles flow, and diamonds are varied overall fluidization flow.

average CO_2 concentration at LSV1 varies from 0.104 to 0.23 with the VD for different fluidization velocities, whereas the variation is from 0.066 to 0.41 without the VD. The presence of CO_2 in this position without VD can only be attributed to back-mixing. Therefore, it can be concluded that no significant leakage of gas below the underwear of the VD was seen, and that the low concentrations seen in the lower-level sampling positions are likely explained mostly by back-mixing.

Declaration of Competing Interest

We, the authors of the manuscript, declare that we have no known competing financial interests or personal relationships that represents a conflict of interest in connection with the work submitted.

Acknowledgements

This work was funded by the Swedish Energy Agency, project number 46626-1.

References

[1] J. Adánez, A. Abad, Chemical-looping combustion: status and research needs, Proc. Combust. Inst. 37 (2019) 4303–4317.
[2] V. Masson-Delmotte, P. Zhai, H.-O. Pörtner, IPCC, 2018: summary for policymakers, in: Global Warming of 1.5°C. An IPCC Special Report on the Impacts of Global Warming of 1.5°C Above Pre-industrial Levels and Related Global Greenhouse Gas Emission Pathways, in the Context of Strengthening the Global Response to the Threat of Climate Change, Sustainable Development, and Efforts to Eradicate Poverty, 2018. In Press.
[3] C. Linderholm, A. Lyngfelt, A. Cuadrat, E. Jerndal, Chemical-looping combustion of solid fuels – operation in a 10 kW unit with two fuels, above-bed and in-bed fuel feed and two oxygen carriers, manganese ore and ilmenite, Fuel 102 (2012) 808–822.

[4] A. Lyngfelt, Chemical looping combustion: status and development challenges, Energy Fuel 34 (2020) 9077–9093.
[5] M. Kramp, A. Thon, E.-U. Hartge, S. Heinrich, J. Werther, Carbon stripping – a critical process step in chemical looping combustion of solid fuels, Chem. Eng. Technol. 35 (2012) 497–507.
[6] H. Sun, M. Cheng, D. Chen, L. Xu, Z. Li, N. Cai, Experimental study of a carbon stripper in solid fuel chemical looping combustion, Ind. Eng. Chem. Res. 54 (2015) 8743–8753.
[7] H. Sun, M. Cheng, Z. Li, N. Cai, Riser-based carbon stripper for coal-fueled chemical looping combustion, Ind. Eng. Chem. Res. 55 (2016) 2381–2390.
[8] N. Berguerand, A. Lyngfelt, Design and operation of a 10 kWth chemical-looping combustor for solid fuels – testing with South African coal, Fuel 87 (2008) 2713–2726.
[9] C. Linderholm, M. Schmitz, P. Knutsson, M. Källén, A. Lyngfelt, Use of low-volatile solid fuels in a 100 kW chemical-looping combustor, Energy Fuel 28 (2014) 5942–5952.
[10] H. Chen, M. Cheng, L. Liu, Y. Li, Z. Li, N. Cai, Coal-fired chemical looping combustion coupled with a high-efficiency annular carbon stripper, Int. J. Greenhouse Gas Control 93 (2020) 102889.
[11] I. Gogolev, A.H. Soleimanisalim, C. Linderholm, A. Lyngfelt, Commissioning, performance benchmarking, and investigation of alkali emissions in a 10 kWth solid fuel chemical looping combustion pilot, Fuel 287 (2021) 119530.
[12] D. Mei, C. Linderholm, A. Lyngfelt, Performance of an oxy-polishing step in the 100 kWth chemical looping combustion prototype, Chem. Eng. J. 409 (2021) 128202.
[13] A. Lyngfelt, B. Leckner, A 1000 MWth boiler for chemical-looping combustion of solid fuels – discussion of design and costs, Appl. Energy 157 (2015) 475–487.
[14] H. Gu, L. Shen, J. Xiao, S. Zhang, T. Song, Chemical looping combustion of biomass/coal with natural iron ore as oxygen carrier in a continuous reactor, Energy Fuel 25 (2011) 446–455.
[15] T. Mendiara, A. Abad, L.F. de Diego, F. García-Labiano, P. Gayán, J. Adánez, Biomass combustion in a CLC system using an iron ore as an oxygen carrier, Int. J. Greenhouse Gas Control 19 (2013) 322–330.
[16] F. Miccio, A. Natali Murri, E. Landi, Synthesis and characterization of geopolymer oxygen carriers for chemical looping combustion, Appl. Energy 194 (2017) 136–147.
[17] C. Linderholm, M. Schmitz, P. Knutsson, A. Lyngfelt, Chemical-looping combustion in a 100-kW unit using a mixture of ilmenite and manganese ore as oxygen carrier, Fuel 166 (2016) 533–542.
[18] J. Wang, H. Zhao, Evaluation of CaO-decorated Fe2O3/Al2O3 as an oxygen carrier for in-situ gasification chemical looping combustion of plastic wastes, Fuel 165 (2016) 235–243.
[19] A. Lyngfelt, A. Brink, Ø. Langørgen, T. Mattisson, M. Rydén, C. Linderholm, 11,000 h of chemical-looping combustion operation—where are we and where do we want to go? Int. J. Greenhouse Gas Control 88 (2019) 38–56.
[20] T. Mattisson, A. Lyngfelt, H. Leion, Chemical-looping with oxygen uncoupling for combustion of solid fuels, Int. J. Greenhouse Gas Control 3 (2009) 11–19.
[21] H. Leion, T. Mattisson, A. Lyngfelt, Using chemical-looping with oxygen uncoupling (CLOU) for combustion of six different solid fuels, Energy Proc. 1 (2009) 447–453.
[22] M. Arjmand, A.-M. Azad, H. Leion, A. Lyngfelt, T. Mattisson, Prospects of Al_2O_3 and $MgAl_2O_4$-supported CuO oxygen carriers in chemical-looping combustion (CLC) and chemical-looping with oxygen uncoupling (CLOU), Energy Fuel 25 (2011) 5493–5502.
[23] P. Gayán, I. Adánez-Rubio, A. Abad, L.F. de Diego, F. García-Labiano, J. Adánez, Development of Cu-based oxygen carriers for chemical-looping with oxygen uncoupling (CLOU) process, Fuel 96 (2012) 226–238.
[24] M. Arjmand, M. Keller, H. Leion, T. Mattisson, A. Lyngfelt, Oxygen release and oxidation rates of $MgAl_2O_4$-supported CuO oxygen carrier for chemical-looping combustion with oxygen uncoupling (CLOU), Energy Fuel 26 (2012) 6528–6539.
[25] A. Shulman, E. Cleverstam, T. Mattisson, A. Lyngfelt, Manganese/iron, manganese/nickel, and manganese/silicon oxides used in chemical-looping with oxygen uncoupling (CLOU) for combustion of methane, Energy Fuel 23 (2009) 5269–5275.
[26] G. Azimi, H. Leion, T. Mattisson, A. Lyngfelt, Chemical-looping with oxygen uncoupling using combined Mn-Fe oxides, testing in batch fluidized bed, Energy Procedia 4 (2011) 370–377.
[27] G. Azimi, H. Leion, M. Rydén, T. Mattisson, A. Lyngfelt, Investigation of different Mn–Fe oxides as oxygen carrier for chemical-looping with oxygen uncoupling (CLOU), Energy Fuel 27 (2013) 367–377.
[28] A. Natali Murri, F. Miccio, V. Medri, E. Landi, Geopolymer-composites with thermomechanical stability as oxygen carriers for fluidized bed chemical looping combustion with oxygen uncoupling, Chem. Eng. J. 393 (2020) 124756.
[29] E.R. Stobbe, B.A. de Boer, J.W. Geus, The reduction and oxidation behaviour of manganese oxides, Catal. Today 47 (1999) 161–167.
[30] P. Moldenhauer, M. Rydén, T. Mattisson, A. Lyngfelt, Chemical-looping combustion and chemical-looping with oxygen uncoupling of kerosene with Mn- and Cu-based oxygen carriers in a circulating fluidized-bed 300W laboratory reactor, Fuel Process. Technol. 104 (2012) 378–389.
[31] I. Adánez-Rubio, P. Gayán, A. Abad, L.F. de Diego, F. García-Labiano, J. Adánez, Evaluation of a spray-dried $CuO/MgAl_2O_4$ oxygen carrier for the chemical looping with oxygen uncoupling process, Energy Fuel 26 (2012) 3069–3081.
[32] C. Kuang, S. Wang, M. Luo, J. Cai, J. Zhao, Investigation of CuO-based oxygen carriers modified by three different ores in chemical looping combustion with solid fuels, Renew. Energy 154 (2020) 937–948.
[33] J. Dai, K.J. Whitty, Impact of fuel-derived chlorine on CuO-based oxygen carriers for chemical looping with oxygen uncoupling, Fuel 263 (2020) 116780.
[34] A. Abad, P. Gayán, R. Pérez-Vega, F. García-Labiano, L.F. de Diego, T. Mendiara, M.T. Izquierdo, J. Adánez, Evaluation of different strategies to improve the efficiency of coal conversion in a 50 kWth chemical looping combustion unit, Fuel 271 (2020) 117514.
[35] M. Fiorentino, A. Marzocchella, P. Salatino, Segregation of fuel particles and volatile matter during devolatilization in a fluidized bed reactor—II. Experimental, Chem. Eng. Sci. 52 (1997) 1909–1922.
[36] G. Bruni, R. Solimene, A. Marzocchella, P. Salatino, J.G. Yates, P. Lettieri, M. Fiorentino, Self-segregation of high-volatile fuel particles during devolatilization in a fluidized bed reactor, Powder Technol. 128 (2002) 11–21.
[37] I. Petersen, J. Werther, Three-dimensional modeling of a circulating fluidized bed gasifier for sewage sludge, Chem. Eng. Sci. 60 (2005) 4469–4484.
[38] D. Kunii, O. Levenspiel, Chapter 9 - solid movement: mixing, segregation, and staging, in: D. Kunii, O. Levenspiel (Eds.), Fluidization Engineering (Second Edition), Butterworth-Heinemann, Boston, 1991, pp. 211–235.
[39] L. Massimilla, H.F. Johnstone, Reaction kinetics in fluidized beds, Chem. Eng. Sci. 16 (1961) 105–112.
[40] D. Kunii, O. Levenspiel, CHAPTER 4 - the dense bed: distributors, gas jets, and pumping power, in: D. Kunii, O. Levenspiel (Eds.), Fluidization Engineering (Second Edition), Butterworth-Heinemann, Boston, 1991, pp. 95–113.
[41] A. Svensson, F. Johnsson, B. Leckner, Bottom bed regimes in a circulating fluidized bed boiler, Int. J. Multiphase Flow 22 (1996) 1187–1204.
[42] M. Hertzberg, H. Schreuder, Role of atmospheric carbon dioxide in climate change, Energy Environ. 27 (2016) 785–797.
[43] F. Johnsson, S. Andersson, B. Leckner, Expansion of a freely bubbling fluidized bed, Powder Technol. 68 (1991) 117–123.
[44] J. Xiang, Q. Li, Z. Tan, Y. Zhang, Characterization of the flow in a gas-solid bubbling fluidized bed by pressure fluctuation, Chem. Eng. Sci. 174 (2017) 93–103.